Title

Spectral Slope and Coherence Quantitatively Summarize Nested Topographic Variability Patterns in Rivers

Authors

Lee, A
Lane, B
Pasternack, GB

Publication Date

2025

DOI

10.1002/rra.4437

Spectral Slope and Coherence Quantitatively Summarize Nested Topographic Variability Patterns In Rivers

A. Lee[1*], B. Lane[1], and G. B. Pasternack[2]

[1]Department of Civil and Environmental Engineering, Utah State University; Logan, UT 84322, USA.

[2]Department of Land, Air & Water Resources, University of California, Davis; Davis, CA 95616, USA.

[*]Corresponding author: Anzy Lee (anzy.lee@usu.edu)

Key Points:

- This study examined the spectral scaling, coherence and cross-phase spectrum of riverbed elevation and width variability for 35 sites across channel types and flow stages.
- Uniform channels had the mildest spectral slope for bed elevation variability, while confined channels had the mildest spectral slope for width variability.
- Braided channels showed the steepest spectral slopes for both bed elevation and width variability.
- Harmonic components of detrended width and bed elevation series mostly exhibited in-phase relationships at bankfull and flood stage across frequencies whereas some out-of-phase relationships were observed at baseflow stage for low frequencies.
- Bed variability spectral slope and mean wetted width were positively correlated across flow stages.

Abstract

Rivers exhibit self-similarity, or spectral scaling, across a wide range of spatial scales, from clusters of individual sediment grains to periodic features such as ripples, dunes, and meanders, extending to entire river valleys and networks. Previous studies have identified relationships between reaches characterized by specific wavelet scales and distinct morphological units or valley controls. Drawing on available high-resolution lidar-based bathymetries of 35 channel reaches, this study investigates linkages between spectral analysis measures and established channel typologies and morphological attributes across diverse river settings. We use spectral analysis to demonstrate how sub-reach scale topographic variability patterns vary by flow stage and channel type. Uniform channels had the mildest spectral slopes for bed elevation variability, while confined channels had the mildest spectral slopes for width variability. In contrast, braided channels had the steepest spectral slopes for both bed and width variability. Coherence analysis revealed that the harmonic components of bed and width are largely in-phase (i.e., when the bed is high, the channel is wide) at bankfull and flood stage, but some out-of-phase relationships were found at baseflow within the low-frequency range. Finally, the longitudinal bed elevation series exhibited steeper spectral slopes with increasing mean wetted width across channel types and flow stages. Our findings on spectral slope and coherence of bed and width undulations may help improve the representation of the nested structure of a river's terrain and variability at different scales from sub-reach to watershed.

1 Introduction

There is an established need to move beyond the central tendencies of channel reach morphology to understand patterns of sub-reach scale topographic variability (White et al., 2010; Wyrick & Pasternack, 2016; Lane et al., 2017; Duffin et al., 2021). Descriptive river reach typologies distinguish both reach-average (e.g., bankfull width) and sub-reach-scale geomorphic features and repeating patterns. For instance, Montgomery and Buffington (1993) distinguish channel types such as pool-riffle, plane-bed and step-pool in part based on observable longitudinal undulations in channel bed elevation and width that result in distinct types and spacing of landforms. These descriptive typologies facilitate the identification of river reaches with different dominant geomorphic features, processes and aquatic habitat conditions. However, none systematically and quantitatively describe or differentiate the entire, nested structure of a river's terrain and variability. A key step to understanding rivers lies in linking reach-scale channel typologies and attributes to multi-scale variability patterns as quantitatively summarized by frequency domain measures.

1.1 Previous Studies on Multiscale Sub-Reach Scale Variability

Longitudinal variations in channel topography, such as in channel width and bed elevation, can contain stochastic non-periodic fluctuations. However, they are highly organized and interrelated to a large degree (Brown & Pasternack, 2017; Palucis & Lamb, 2017; Pasternack et al., 2018a, 2018b) owing to their lability and tendency for mutual adjustment to external forcing (Hack, 1960). As a result, rivers exhibit self-similarity, or spectral scaling, over scales ranging from the size of clusters of individual sediment grains to periodic structures such as ripples, dunes, and meanders to entire river valleys and networks (Figure 1) (Nikora & Hicks, 1997; Turcotte, 1997; Rodriguez-Iturbe & Rinaldo, 2001). Here, we define sub-reach scale topographic variability (SRV) as the nested patterns of topographic (co)variability along a river ranging from the particle (10^{-2}-10^{0} channel width) to reach (10^{2}-10^{3} channel width) scales. SRV acts as a major control on river hydrodynamics via topographic steering, the morphological control of water depth, speed and direction (Sear, 1996; MacWilliams et al., 2006; Blanckaert, 2010; Huang et al., 2004). That in turn affects river processes including sediment transport (Sear, 1996), hyporheic exchange (Lee et al., 2020), and geochemical cycling (Movahedi et al., 2021) as well as aquatic habitat structure (Wheaton et al., 2010; Lane et al., 2018; Dudunake et al., 2020).

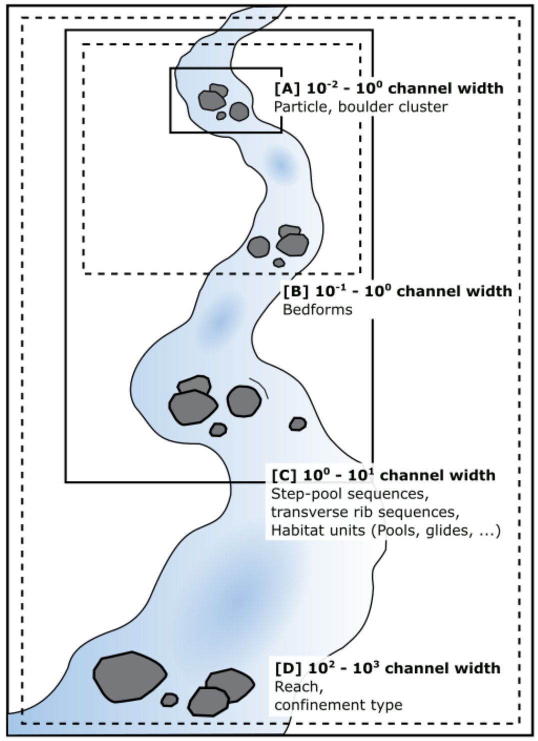

Figure 1. River sub-reach-scale topographic variability is the totality of everything in this figure.

Past studies have observed distinct patterns of SRV at different spatial scales. For example, the longitudinal spacing of sediment clusters (Hassan & Reid, 1990) and ripples (Davies, 1980) (relative to roughness height) has been shown to be repeating at wavelengths 10^{-2}-10^{0} channel width and as a function of flow resistance (A in Figure 1). Bedform scale variability (B in Figure 1) can exhibit multiscale structures (Nikora & Hicks, 1997; Coleman & Nikora, 2011; Martin & Jerolmack, 2013) with a range of wavelengths (10^{-1}-10^{0} channel width) and heights (Hino, 1968; Nikora et al., 1997; van der Mark et al., 2008; McElroy & Mohrig, 2009; Signh et al., 2011). At the morphological unit scale (10^{0}-10^{1} channel width, C in Figure 1), pool spacing in riffle-pool reaches has been observed to range from fit to seven bankfull widths in small pools and 30-40 bankfull widths in large pools (Duffin et al., 2021; Gibson et al. 2019; Keller & Melhorn 1978; Leopold et al., 1964).

Several broad approaches exist to quantify SRV in rivers for different applications. These include classic statistical descriptions such as root mean square deviation (Glenn et al., 2006; Frankel & Dolan, 2007), geostatistics such as variogram/autocorrelation analysis (Legleiter, 2014), object-oriented analysis describing the longitudinal sequencing of features which is useful in data-limited systems (Hay et al., 2001; Halwas & Church, 2002), covariance of longitudinal series of channel features (e.g., width, bed elevation, originating in Brown & Pasternack, 2014, 2017; Nogueira et al., 2024) and frequency domain or spectral analysis (Nikora & Hicks, 1997; McKean et al., 2008; Duffin et al., 2021). Among these approaches, in data-rich systems, spectral analysis can capture the scale dependence and covariance inherent in landforms by deconstructing patterns and quantifying variability at many, nested spatial scales. The application of spectral analysis to river topography is also flow independent, objective, repeatable, and does not require intensive field surveying.

Past studies of river SRV patterns have shown that the power spectrum may be fit with a power law where its slope (i.e., spectral slope) represents the relative balance between low- and high-frequency undulations in the channel terrain, defined as spectral scaling (Burrough, 1981; Clifford et al., 1992; Pelletier, 2007; Williams et al., 2019). Nikora (1991) found a relation between sinuosity and the spectral slope of river channel width for 46 river reaches in Moldavia with different planform patterns. Duffin et al. (2021) used continuous wavelet analysis of channel terrain data to identify reaches with distinct dominant morphological units (e.g., riffle-pool from glide) as well as individual morphological units (e.g., pools) for three small pool-riffle reaches in Idaho. They observed some, but limited, relationships between reaches dominated by certain wavelet scales (e.g., low-frequency bed elevation undulations) and distinct morphological units and valley controls. However, more research is needed to explore linkages between spectral analysis measures and established channel typologies and morphological attributes across diverse river settings.

1.2 Conceptual Model and Scientific Questions

When considering the longitudinal series of mean-width-normalized wetted width (Wn) and detrended, mean-width-normalized bed elevation (Zn), we expect river reaches with steeper spectral slopes of Wn and Zn (Figure 2a, red line) to undulate longitudinally but to do so relatively smoothly, because low-frequency SRV patterns (i.e., larger repeating geomorphic features) dominate (Figure 2b,d). In contrast, we expect river reaches with gentler spectral slopes (Figure 2a, blue line) to be associated with a greater degree of high-frequency topographic variability, because there is a similar amount of spectral power across all spatial scales (Figure 2c,e). To test this expectation, we first ask [Q1] how the spectral slopes of Zn and Wn series vary as a function of channel type.

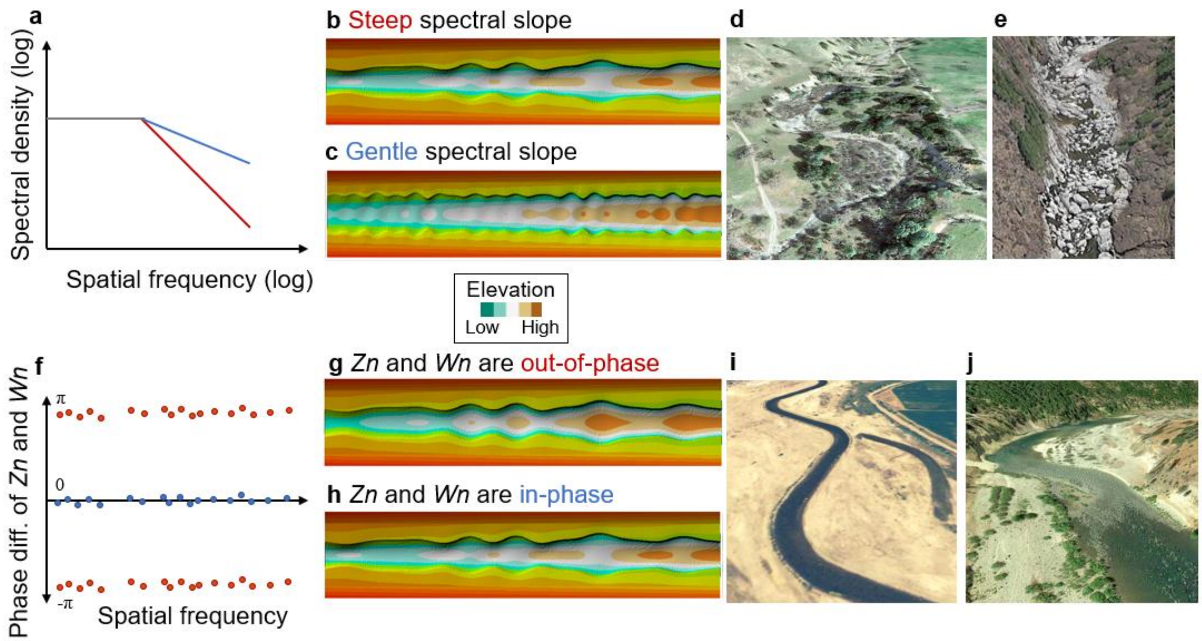

Figure 2. Proposed conceptual model of end-member river reaches with different spectral properties. (a) Spectral density plot with a steep spectral slope (red line) and gentle spectral slope (blue line), (b and d) a channel terrain model and representative river topography with a steep spectral slope of Zn and Wn series, (c and e) a channel terrain model and representative river topography with a gentle spectral slope of Zn and Wn series, (f) phase difference of Zn and Wn series: out-of-phase (π or – π, red dots), in-phase (0, blue dots) (g and i) a channel terrain model and representative river topography having out-of-phase relationship between Zn and Wn series, and (h and j) a channel terrain model and representative river topography having in-phase relationship between Zn and Wn series.

In addition to the spectral slope, the phase difference between two series, a value between 0 and π, is another spectral property that identifies how far apart two series are on their paths of undulation for a given frequency. Zn and Wn are considered in-phase (i.e., when the bed is high, the channel is wide) (Figure 2g,i) if their phase difference is close to zero (Figure 2f, blue dots). On the other hand, Zn and Wn are considered out-of-phase (i.e., when the bed is high, the channel is narrow) (Figure 2h,j) if their phase difference is close to π or - π (Figure 2f, red dots). Building on past research showing that, in many individual rivers, bed and width undulations are linked (Brown and Pasternack, 2017; Nogueira et al., 2024), we further ask [Q2] how Zn and Wn undulations align based on their phase differences across flow stages and channel types.

Finally, building on previous research that links bankfull width to SRV patterns in channel bed elevation (e.g., bedforms and pool-riffle spacing) (Leopold et al., 1964), we expect the channel width and the spectral slope of Zn representing bed variability to be related. For example, for single-threaded alluvial rivers, increasing width is hypothesized to be associated with increasing spectral slope because larger rivers become dominated by a single spatial scale of topographic undulation dictated by meandering. Here, we further ask [Q3] if mean wetted width or other reach-scale channel attributes typically used in channel classification are related to the spectral slopes of Zn and Wn.

2 Study Area and Methods

2.1 Study Area and Data Processing

The study area consists of 35 ephemeral river reaches along the southern Pacific coastline of California, USA (Figure 3), spanning coastal valleys, foothills, and rugged mountains with significant geologic diversity but generally similar physiographic characteristics. These study reaches fall within five channel types (six to eight study reaches per channel type) identified for the South Coast region as detailed in Byrne et al. (2020) and Lane et al. (2021) based on an equal effort stratified-random sampling strategy and multivariate analysis of the resulting 67 surveyed reaches. The five channel types are: (1) unconfined, uniform, sand-gravel, (2) partly-confined, braided, gravel-cobble, (3) confined, Cascade/step-pool, cobble-boulder, (4) confined, uniform, gravel-cobble, and (5) confined, riffle-pool, gravel-cobble channel. Details on how channel types were determined are available in Supporting Information: Text S1. Fifteen reach-scale channel attributes were previously calculated for each study reach, as detailed in Nogueira et al. (2024): stream order, catchment area, valley confinement, channel slope, coefficient of variance of width and depth at bankfull stage, and average baseflow/bankfull/flood stage width, water depth, and width-to-depth ratio. The calculation methods and channel attribute values are provided in Table S2.

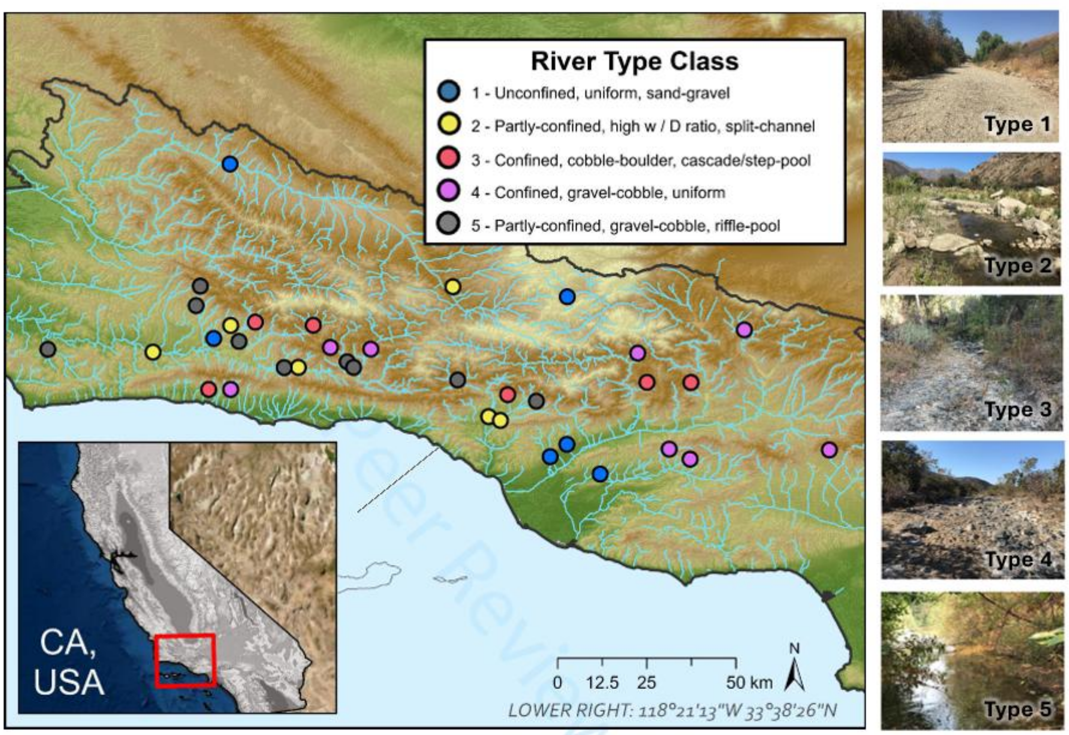

Figure 3. Map of the California South Coast showing all 35 study reaches color-coded by channel type and representative photos for each channel type. The five channel types are: (1) unconfined, uniform, sand-gravel, (2) partly-confined, braided, gravel-cobble, (3) confined, cascade/step-pool, cobble-boulder, (4) confined, uniform, gravel-cobble, and (5) confined, riffle-pool, gravel-cobble channel (reproduced from Nogueira et al. 2024 with permission).

The bare-ground elevation point cloud data for each study reach was clipped and processed to obtain a meter-resolution raster digital elevation model of the dry river-corridor reach. Longitudinal Wn and Zn series were extracted for selected elevations representing key flow stages (Nogueira et al., 2024). Further information on geomorphic analysis including the key metrics of LiDAR project data (Table S1) and the final yes/no classification tree (Figure S1) can be found in Supporting Information: Text S2.

2.2 Data Analysis

To answer the scientific questions posed above, we performed spectral analysis on Wn and Zn for each of the 35 study reaches across three key flow stages: baseflow, bankfull, and flood stage. Q1 was answered by comparing the site-specific spectral slopes of Zn and Wn within and between channel types, and relative to the conceptual model to see if the model held up.

To answer Q2, we first identified frequencies with statistically significant coherence (p = 0.01) between Zn and Wn, and then evaluated the distribution of phase differences of coherent frequencies (i.e., phase of cross-spectrum). Coherence ($C_{xy}(f)$) represents the normalized cross-correlation between Zn and Wn at a given frequency (f) as defined below, ranging from 0 (not coherent) to 1 (high coherency):

$$C_{xy}(f) = \frac{|G_{xy}(f)|^2}{G_{xx}(f)G_{yy}(f)} \quad \text{Eq. 1}$$

where $G_{xy}(f)$ is the cross-spectral density between *x* and *y* for a given frequency *f*, and $G_{xx}(f)$ and $G_{yy}(f)$ are the auto-spectral density of *x* and *y*, respectively (Bendat & Piersol, 2011). The phase of cross-spectrum of Zn and Wn was then evaluated across flow stages and frequencies using scatterplots and kernel density plots.

Finally, Q3 was answered by assessing multi-site relationships (R^2 of fitted power functions) between stage-specific spectral slopes of Wn and Zn and each of the 15 reach-scale channel attributes. Detailed information on spectral and coherence analysis is given in Supporting Information: Text S2, and MATLAB scripts are available at https://github.com/anzylee/Spectral_Analysis_GCS_public.

3 Results

3.1 Spectral Slopes by Channel Type

With respect to Q1, the site-specific spectral slopes of Zn and Wn varied as a function of channel type for different flow stages. Table 1 presents the average spectral slope for various flow stages and channel types, and Figure S3 shows box plots of Zn and Wn spectral slopes with respect to channel type. For all channel types, the channel type-average spectral slopes of Zn and Wn became steeper as flow stage increased (by an average of 61.2% and 61.5%, respectively, from baseflow to flood). When considering the Zn series, study reaches classified as partly-confined braided channels (channel type 2) exhibited the steepest spectral slopes, whereas unconfined uniform channels (channel type 1) exhibited the mildest spectral slopes, followed by confined uniform channels (channel type 4) for all flow stages (Table 1, Figure S3). When considering the Wn series, partly-confined braided channels again exhibited the steepest spectral slopes among all channel types whereas confined channels (channel type 3 and 4) exhibited milder slopes for bankfull and flood and followed by unconfined uniform sand-gravel channels (channel type 1) which had the mildest slope for baseflow. The site-specific spectral slope values for Wn and Zn for baseflow, bankfull, and flood stages are provided in Table S4.

Table 1. For both mean-width-normalized wetted width (Wn) and detrended, mean-width-normalized bed elevation (Zn), at each stage, numbers indicate the channel type ordered from steepest (first column) to mildest (last column) spectral slope, with each channel type's average spectral slope in parentheses. Channel type numbering is the same as in Figure 3.

Variable	**Stage**	**← Steeper**				**Milder →**
	Baseflow	2 (1.31)	3 (1.11)	4 (1.03)	5 (0.98)	1 (0.64)
Zn	Bankfull	2 (1.55)	5 (1.24)	3 (1.18)	4 (1.08)	1 (1.03)
	Flood	2 (1.93)	5 (1.65)	1 (1.60)	4 (1.28)	3 (1.28)
	Baseflow	2 (1.45)	3 (1.35)	4 (1.32)	5 (1.18)	1 (1.03)
Wn	Bankfull	2 (1.70)	5 (1.68)	1 (1.64)	4 (1.59)	3 (1.50)
	Flood	2 (2.25)	5 (2.11)	1 (2.05)	3 (1.84)	4 (1.82)

3.2 Bed and Width Undulation Coherent Phasing

Figure 4 addressed Q2 by showing the scatter plots of phase differences between Zn and Wn for coherent frequencies at three key flow stages for (a) all channel types and (b-f) each channel type. As visualized by the kernel density plots, the median phase differences were 0.04 (2.3°), 0.01 (0.6°), and 0.01 rad (0.6°) and the standard deviations of phase differences were 1.31 (75°), 0.49 (28°), and 0.35 rad (20°) for baseflow, bankfull and flood stage, respectively, across channel types (Figure 4a). At bankfull and flood stage, the median phase difference between Zn and Wn was close to 0, indicating an in-phase relationship, with a standard deviation of 0.49

(28°) and 0.35 rad (20°), respectively, across channel types. At baseflow stage, the standard deviation of phase differences was larger than those at bankfull and flood stages due to the out-of-phase relationships between Zn and Wn within the low-frequency range (Figure 4a, blue density plot on the left and blue dots). This out-of-phase relationship of low-frequency Zn and Wn was observed in most channel types (Figure 4c-f), except for channel type 1 (Figure 4b).

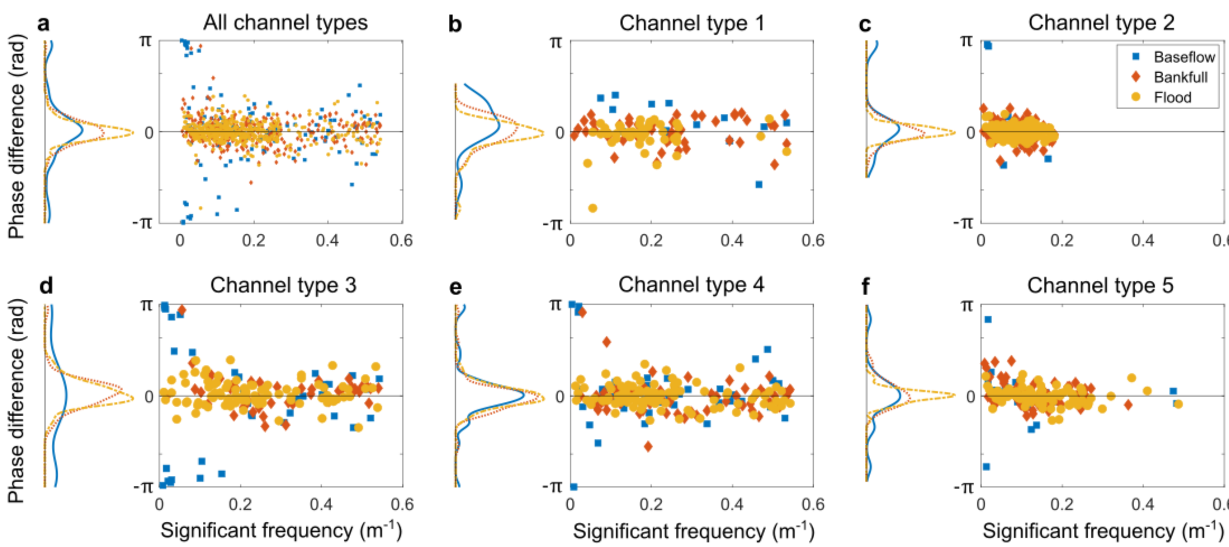

Figure 4. Scatter plots and kernel density plots (to left) of phase differences between Zn and Wn for coherent frequencies at baseflow (blue squares), bankfull (orange diamonds), and flood (yellow dots) stages for (a) all channel types, (b-f) channel type 1-5 where channel type numbering is the same as in Figure 3. The horizontal solid line denotes a phase difference of 0 indicating an in-phase relationship.

Here, we examine individual sites exhibiting extreme topographic states to help understand the results for Q1 and Q2 relative to the conceptual model. Figure 5 illustrates (a and f) wetted polygons, (b and g) Zn (mean-width-normalized bed elevation) series, (c and h) Wn (mean-width-normalized wetted width) series, (d and i) the most dominant harmonic components of Zn, and (e and j) the most dominant harmonic components of Wn for two example sites. The harmonic analysis was performed using the `numpy.fft.fft` function from Numpy (Harris et al., 2020). The first example site, classified as channel type 1 (Figure 5a-e, unconfined, uniform, sand-gravel) with a bankfull width of 38 m, has some of the mildest baseflow Zn and Wn spectral slopes of any study site (0.6 and 1.03, respectively, Table 1). The second example site, classified as channel type 2 (Figure 5f-j, partly confined, braided, gravel-cobble) with a bankfull width of 244 m, has some of the steepest flood stage Zn and Wn spectral slopes (1.93 and 2.25, respectively, Table 1). The first example site exhibits out-of-phase relationships between the two lowest-frequency harmonic components of Zn (1, 2, and 4 in Figure 5d) and Wn (1, 2, and 4 in Figure 5e), which further supports Q2 results. For the second site, the harmonic components of Zn and Wn are mostly in-phase (Figure 5i,j). The lowest-frequency component (1, orange line) exhibits the largest phase difference of 0.97 rad (55.8°).

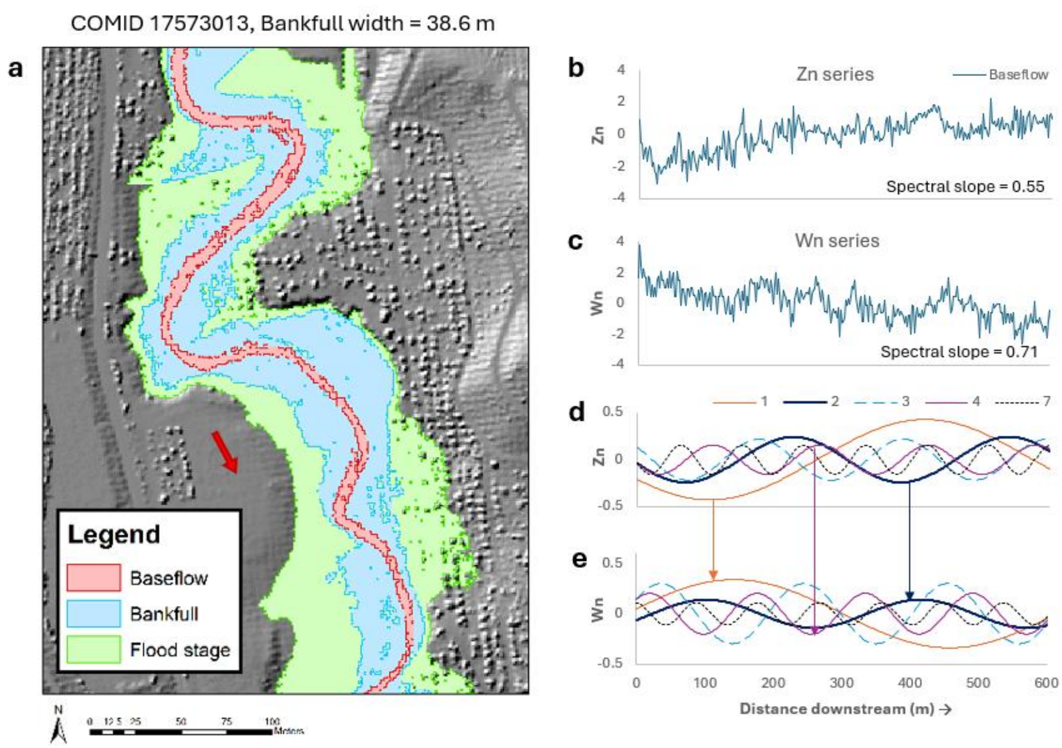

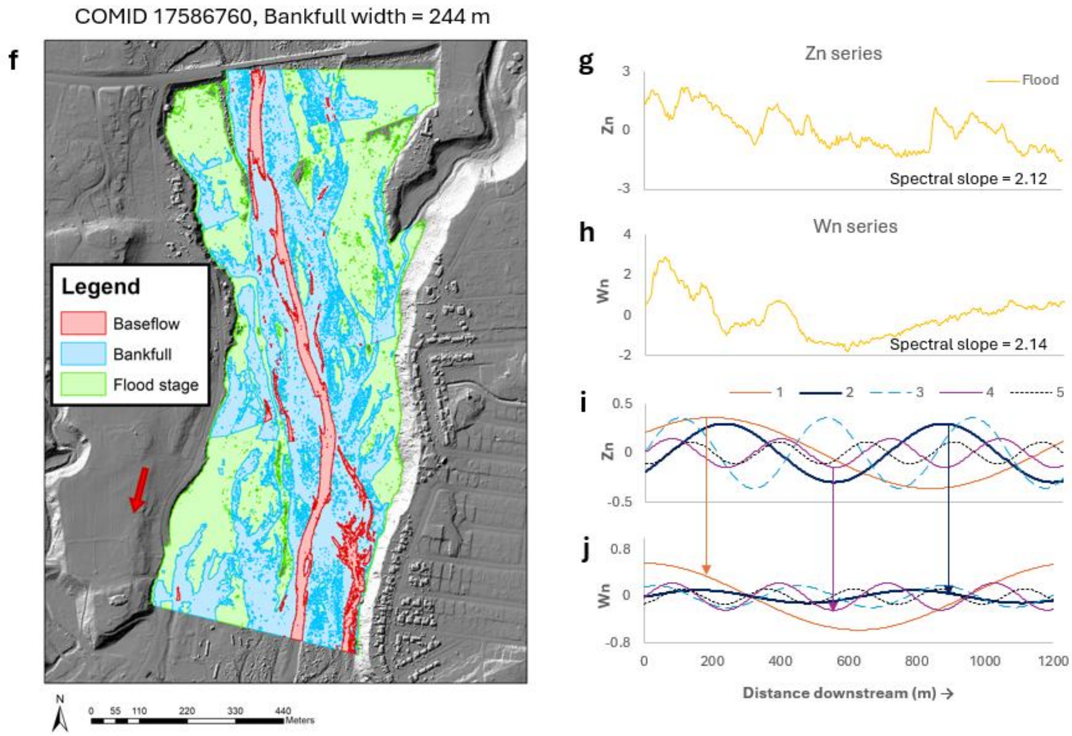

Figure 5. Wetted polygons (a and f), Zn (mean-width-normalized bed elevation) series (b and g), Wn (mean-width-normalized wetted width) series (c and h), the most dominant harmonic components of Zn (d and i) and Wn (e and j) for two example sites having some of the mildest baseflow Zn and Wn spectral slopes in channel type 1 (Figure 6a-e, unconfined, uniform, sand-gravel) and steepest flood Zn and Wn spectral slopes in channel type 2 (Figure 6f-j, partly confined, braided, gravel-cobble). Bankfull widths and spectral slopes are indicated. The latitude and longitude are (34.3538, -119.104879) and (34.4233, -119.302179) for the first and second site, respectively.

3.3 Spectral Slope Correlations with Conventional Reach Metrics

Regression analysis between the spectral slopes of Zn and Wn and reach-scale channel attributes revealed some but limited relationships. The baseflow Zn spectral slope and baseflow width showed an R^2 of 0.51 (purple dots and dashed line in Figure S4g), the bankfull Zn spectral slope and bankfull width had an R^2 of 0.53 (light-blue dots and dashed line in Figure S4h), and the flood stage Zn spectral slope and floodplain width had an R^2 of 0.72 (brown dots and dashed line in Figure S4i). Looking across flow stages, a positive relationship was observed ($R^2 = 0.7$) between Zn spectral slope and mean wetted width (Figure 6). This relationship is evident in the two example sites in Figure 5, where the first site is narrower (baseflow width = 5.24 m) with milder Zn spectral slope (0.55) and the second site is much wider (flood width = 441 m) with a steeper Zn spectral slope (2.12). On the other hand, the Wn spectral slope was not strongly correlated with any reach-scale channel attributes. Thus, larger channels seem to have more simplified spectra of bed undulations in alignment with expectations but still relatively complex spectra of width undulations contrary to expectations. Additional scatter plots and fitted power functions are depicted in Figure S4.

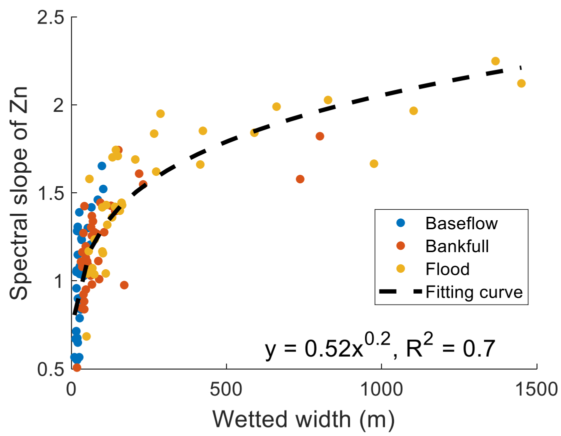

Figure 6. The regression model of spectral slope of Zn versus mean wetted width across 35 study sites and three flow stages. The fitted power function is described by a dashed line and the associated equation and correlation coefficient (R^2) is indicated.

4 Discussion

This study examined the spectral scaling, coherence, and cross-phase spectrum of Zn and Wn for 35 river reaches spanning five channel types with flashy ephemeral flow regimes. While spectral analysis has been used to examine topographic variability in river channels, there has not been a comprehensive study linking the spectral slopes of Zn and Wn to specific channel types or reach-scale channel attributes. Additionally, instead of focusing solely on the covariance between Zn and Wn series (Pasternack et al., 2018b; Nogueira et al., 2024) or identifying key scales of variability (McKean et al., 2008; Duffin et al., 2021), this study applies cross-spectrum analysis of Zn and Wn to a large and diverse set of river reaches, offering new insights into how the underlying harmonic components of Zn and Wn relate to each other. Specifically, we found that spectral slopes of Zn and Wn vary with flow stage and channel type in an explainable manner [Q1], Zn and Wn mostly exhibited coherent, in-phase relationships across SRV scales for all stages except low-frequency undulations at baseflow stage [Q2], and the spectral slope of Zn had a positive relationship with mean wetted width across flow stages [Q3].

The finding that spectral slopes of both Zn and Wn generally increased at higher flow stages indicates that low-frequency (larger spatial scale) variations in both attributes become dominant compared to high-frequency (smaller spatial scale) variability patterns as flow stage increases regardless of channel type. This aligns with channel and valley walls and large bedrock features acting as dominant topographic controls on hydrodynamics at higher flows, while smaller features (e.g., boulder clusters, bedforms, morphological units, Figure 1) associated with high-frequency variability are more dominant controls at low flows (MacVicar & Roy, 2007; Sawyer et al., 2010; Pasternack et al., 2018b; Kalathil & Chandra, 2021).

Differences in the spectral slopes between channel types can be understood in terms of their dominant SRV patterns. The dominance of low-frequency Zn variations in braided channels resulted in steeper spectral slopes, whereas the lack of low-frequency Zn variations in uniform channels yielded milder spectral slopes; in other words, uniform channels do not have meanders, riffles, and pools generating high bed relief at low frequencies, but instead have plane beds. This finding is consistent with Duffin et al.'s (2021) finding that river reaches containing the most pronounced SRV patterns and largest bed features exhibited the highest wavelet power across scales. For Wn, partly-confined braided channels again yielded the steepest spectral slopes among all channel types, whereas confined channels (channel types 3 and 4) resulted in milder slopes, as their width variability is constrained by valley walls limiting low-frequency undulations. Across stages, even though braided rivers exhibit significant complexity in their wetted area polygons at bankfull stage (Figure 5f), their Wn spectral slopes are not particularly mild, as medium to low-frequency undulations exhibit substantial spectral density. This observation is consistent with our finding that steepening of Wn spectral slope is driven by a gain in low frequency undulations rather than a loss of high-frequency undulations as stage increases (e.g., flood Wn is controlled by valley scale). In other words, as stage increases, the water increasingly interacts with valley walls and terraces that have high-amplitude low-frequency undulations. For a given stage, Wn spectral slope gets steeper as wetted width increases (Table 1) and this can be due to a strong link between width and meander wavelength– the bigger a river gets, the more it meanders (Williams, 1986; Hickin, 1978). More broadly, our findings suggest that the spectral properties of Zn and Wn offer an equivalent way to describe topographic patterning in rivers on par with descriptive channel typologies, with the advantage of being more compact, quantitative, and free of language misinterpretations. While this study mainly focused on the variations in spectral slope, future research could explore the area under the spectral density curve (Figure 2a) as it represents the integrated energy over a range of frequencies and could provide valuable insights into surface roughness characteristics (Burrough, 1983; Huang and Bradford, 1992).

Coherence analysis showed that, for a large set of geomorphologically diverse river reaches, Zn and Wn are mostly in-phase across frequencies for bankfull and flood conditions. The in-phase covariance structure of Zn and Wn for bankfull and flood can be explained by the local narrowing/widening of a channel causing flow acceleration/deceleration and riverbed grain entrainment/deposition (Chartrand et al., 2018). Pasternack et al. (2018a) demonstrated that bed and width are positively covary at morphodynamically relevant water stages where the topography and large bed element structure are set. On the other hand, we observed out-of-phase relationships (π or $-\pi$) between Zn and Wn in channel types 2-5 for baseflow, which corresponds to either a nozzle (Zn, -Wn) or an oversized (-Zn, Wn). Wiener & Pasternack (2022) suggested that baseflow Zn and Wn are expected to be out-of-phase in many cases, especially in confined and bedrock/boulder streams, because once these landforms and large bed elements are in place, the hydraulics are forced to conform to them at lower flows. In our study, the substrates of the channel types that showed an out-of-phase relationship between Zn and Wn range from gravel to boulder, which are more resistant to hydraulic forcing than sand-gravel channels (channel type 1), resulting in negative covariance between Zn and Wn (Nogueira et al., 2024).

Finally, limited relationships were observed between the spectral slopes of bed and width series and reach-scale channel attributes. The positive relationship between the spectral slope of Zn and mean wetted width indicates that the spacing between repeating bed features like riffles and pools tends to increase with mean channel width. The pool spacing in riffle-pool reaches has been found to range from five to seven bankfull widths (Leopold et al., 1964; Keller, 1971;

Richards, 1976; Gregory et al., 1994). However, some reported that the modes of spacing between riffles and pools ranged from three to five bankfull widths, which is presumably bedform-scale variability (Carling and Orr, 2000). Based on this observation, Wyrick and Pasternack (2014) explored the use of baseflow width as a metric to more accurately describe the longitudinal spacings between channel morphological units and proposed that valley width could potentially serve as a measure for larger-scale bed profile variability. Our study showed a connection between the mean wetted width and the metric describing bed profile variability at the same flow stage (e.g., mean baseflow width and spectral scaling of Zn for baseflow), revealing a power-law relationship across stages. While no other relationships were apparent, study site selection was not set up to address this question (i.e., balanced sampling across channel metric ranges) and additional research could explore connections between established reach-scale channel metrics and the frequency domain metrics considered herein.

Spectral slope may serve as a valuable new river channel attribute to characterize and distinguish multiscale variability of channel topography. Spectral slope is an effective metric to describe nested topographic scaling of SRV across scales and has been shown to be a critical predictor of channel type, independent of traditional terrain metrics such as elevation and curvature. Guillon et al. (2020) found that, in a machine learning approach to predict geomorphic channel types using coarse geospatial predictors, the fractal dimension - directly related to spectral slope - was a stronger predictor of channel type than conventional terrain metrics based on 10-m topographic data. Furthermore, given that over 97% of the world’s rivers have a channel width of less than 30 meters (Downing et al., 2012), our findings provide valuable insights into estimating the spectral scaling and covariance structures of sub-reach variability by leveraging channel and valley characteristics identifiable in 10 m resolution data.

5 Conclusion

Drawing on available high-resolution lidar-based bathymetries of 35 channel reaches, our study investigated the spectral slope and coherence of five different channel types. Across channel types, the longitudinal series of Wn and Zn showed steeper spectral slopes (e.g., low-frequency dominated oscillations) with increasing flow stage. Uniform channels had the mildest spectral slope of Zn, while confined channels had the mildest spectral slope of Wn. In contrast, braided channels showed the steepest spectral slopes of Zn and Wn. Coherence analysis revealed that the harmonic components of bed and width are largely in-phase for bankfull and flood stages, but some out-of-phase relationships were found at baseflow within the low-frequency range. From regression analysis, a relationship between Zn spectral slope and mean wetted width was found across flow stages. This study provides information about spectral scaling and covariance structure of bed and width variability, which may help improve physical understanding and representation of nested sub-reach scale variability patterns that act as a major control on hydrodynamics and river processes. These outcomes could support predictions of hydraulics and aquatic habitat conditions from sub-reach to watershed scales with limited resource requirements.

Acknowledgments

This research was supported by the California State Water Resources Control Board. The authors also acknowledge funding from the Utah Water Research Laboratory and the USDA National Institute of Food and Agriculture, Hatch project numbers #CA-D-LAW-7034-H and CA-D-LAW-2243-H. We thank Kenny Larrieu and Xavier Nogueira for their contributions to the development of geomorphic covariance structure toolsets, visualization, and data process.

Open Research

Topographic datasets and MALTAB codes for spectral analysis, coherence analysis, and regression analysis are available at https://github.com/anzylee/Spectral_Analysis_GCS_public. Geomorphic covariance structure graphical user interface software is available at https://github.com/xaviernogueira/GCS-Analysis-Tools.

References

Bendat, J. S., & Piersol, A. G. (2011). *Random data: analysis and measurement procedures.* John Wiley & Sons, Inc., Hoboken, New Jersey, US.

Blanckaert, K. (2010), Topographic steering, flow recirculation, velocity redistribution, and bed topography in sharp meander bends, *Water Resour. Res.*, 46, W09506, https://doi.org/10.1029/2009WR008303.

Brown, R. A., & Pasternack, G. B. (2014). Hydrologic and topographic variability modulate channel change in mountain rivers. *Journal of Hydrology*, 510, 551-564. https://doi.org/10.1016/j.jhydrol.2013.12.048

Brown, R. A., & Pasternack, G. B. (2017). Bed and width oscillations form coherent patterns in a partially confined, regulated gravel–cobble-bedded river adjusting to anthropogenic disturbances. *Earth Surface Dynamics*, *5*(1), 1-20. https://doi.org/10.5194/esurf-5-1-2017

Burrough, P. A. (1981). Fractal dimensions of landscapes and other environmental data. *Nature*, 294, 240–242. https://doi.org/10.1038/294240a0

Burrough, P. A. (1983). Multiscale sources of spatial variation in soil. I. The application of fractal concepts to nested levels of soil variation. *Journal of soil science*, *34*(3), 577-597. https://doi.org/10.1111/j.1365-2389.1983.tb01057.x

Carling, P., & Orr, H. (2000). Morphology of riffle-pool sequences in the River Severn, England. *Earth Surface Processes and Landforms*, 25(4), 369–384.

Chartrand, S. M., Jellinek, A. M., Hassan, M. A., & Ferrer-Boix, C. (2018). Morphodynamics of a width-variable gravel bed stream: New insights on pool-riffle formation from physical experiments. *Journal of Geophysical Research: Earth Surface*, 123(11), 2735-2766. https://doi.org/10.1029/2017JF004533

Clifford, N. J., Robert, A., & Richards, K. S. (1992). Estimation of flow resistance in gravel-bedded rivers. *Earth Surf. Process. Landf.*, 17, 111–126. https://doi.org/10.1016/0037-0738(93)90074-F

Coleman, S. E., & Nikora, V. I. (2011). Fluvial dunes: Initiation, characterization, flow structure. *Earth Surface Processes and Landforms*, 36, 39–57. https://doi.org/10.1002/esp.2096

Davies, T. R. (1980). Bedform spacing and flow resistance. *Journal of the Hydraulics Division*, *106*(3), 423-433. https://doi.org/10.1061/JYCEAJ.0005384

Downing, J. A., Cole, J. J., Duarte, C. M., Middelburg, J. J., Melack, J. M., Prairie, Y. T., Kortelainen, P., Striegl, R. G., McDowell, W. H., & Tranvik, L. J. (2012). Global abundance and size distribution of streams and rivers. *Inland waters*, 2(4), 229-236. https://doi.org/10.5268/IW-2.4.502

Duffin, J., Carmichael, R. A., Yager, E. M., Benjankar, R., & Tonina, D. (2021) Detecting multi-scale riverine topographic variability and its influence on Chinook salmon habitat selection. *Earth Surf Process Landforms*, 46, 1026–1040. https://doi.org/10.1002/esp.5077.

Dudunake, T., Tonina, D., Reeder, W. J., & Monsalve, A. (2020). Local and reach-scale hyporheic flow response from boulder-induced geomorphic changes. *Water Resources Research*, 56, e2020WR027719. https://doi.org/10.1029/2020WR027719

Frankel, K. L., & Dolan, J. F., (2007). Characterizing arid region alluvial fan surface roughness with airborne laser swath mapping digital topographic data. *J. Geophys. Res.*, 112, F02025. http://dx.doi.org/10.1029/2006JF000644.

Gibson, S., Osorio, A., Creech, C., Amorim, R., Dircksen, M., Dahl, T., & Koohafkan, M. (2019). Two pool-to-pool spacing periods on large sand-bed rivers: Mega-pools on the Madeira and Mississippi. *Geomorphology*, *328*, 196-210. https://doi.org/10.1016/j.geomorph.2018.12.021

Glenn, N. F., Streutker, D. R., Chadwick, D. J., Thackray, G. D., & Dorsch, S. J. (2006). Analysis of LiDAR-derived topographic information for characterizing and differentiating landslide morphology and activity. *Geomorphology*, 73, 131–148. https://doi.org/10.1016/j.geomorph.2005.07.006

Gregory, K.J., Gurnell, A.M., Hill, C.T. and Tooth, S. (1994), Stability of the pool-riffle sequence in changing river channels. Regul. Rivers: Res. Mgmt., 9: 35-43. https://doi.org/10.1002/rrr.3450090104

Guillon, H., Byrne, C. F., Lane, B. A., Sandoval Solis, S., & Pasternack, G. B. (2020). Machine learning predicts reach-scale channel types from coarse-scale geospatial data in a large river basin. *Water Resources Research*, *56*(3), e2019WR026691. https://doi.org/10.1029/2019WR026691

Hack, J.T. (1960). Interpretation of erosional topography in humid temperate regions. *American Journal of Science*, *258*, 80-97.

Halwas, K. L., & Church, M. (2002). Channel units in small, high gradient streams on Vancouver Island, British Columbia. *Geomorphology*, 43(3-4), 243-256. https://doi.org/10.1016/S0169-555X(01)00136-2

Harris, C. R., Millman, K. J., van der Walt, S. J., Gommers, R., Virtanen, P., Cournapeau, D., ... & Oliphant, T. E. (2020). Array programming with NumPy. *Nature*, 585(7825), 357-362. https://doi.org/10.1038/s41586-020-2649-2

Hassan, M. A., & Reid, I. (1990). The influence of microform bed roughness elements on flow and sediment transport in gravel bed rivers. *Earth Surface Processes and Landforms*, *15*(8), 739-750. https://doi.org/10.1002/esp.3290150807

Hay, G. J., Marceau, D. J., Dube, P., & Bouchard, A. (2001). A multiscale framework for landscape analysis: object-specific analysis and upscaling. *Landscape Ecology*, *16*, 471-490. https://doi.org/10.1023/A:1013101931793

Hino, M. (1968). Equilibrium-range spectra of sand waves formed by flowing water. *J. Fluid Mech.*, 34(3), 565–573.

Huang, C. H., & Bradford, J. M. (1992). Applications of a laser scanner to quantify soil microtopography. *Soil Science Society of America Journal*, *56*(1), 14-21. https://doi.org/10.2136/sssaj1992.03615995005600010002x

Huang, H. Q., H. H. Chang, & G. C. Nanson (2004), Minimum energy as the general form of critical flow and maximum flow efficiency and for explaining variations in river channel pattern, *Water Resour. Res.*, 40, W04502, https://doi.org/10.1029/2003WR002539

Keller, E. A. (1971). Areal sorting of bed-load material: The hypothesis of velocity reversal, *Geol. Soc. Am. Bull.*, 82, 753–756. https://doi.org/10.1130/0016-7606(1971)82[753:ASOBMT]2.0.CO;2

Lane, B. A., Pasternack, G. B., Dahlke, H. E., & Sandoval-Solis, S. (2017). The role of topographic variability in river channel classification. *Progress in Physical Geography*, 41(5), 570-600. https://doi.org/10.1177/0309133317718133

Lane, B. A., Pasternack, G. B., & Sandoval-Solis S. (2018) Integrated analysis of flow, form, and function for river management and design testing. *Ecohydrology*, 11, e1969. https://doi.org/10.1002/eco.1969

Lane, B. A., Guillon, H., Byrne, C. F., Pasternack G. B., Rowles, J., & Sandoval-Solis, S. (2021). Channel reach morphology and landscape properties are linked across a large heterogeneous region. *Earth Surface Process and Landforms*. https://doi.org/10.1002/esp.5246

Lee, A., Aubeneau, A. F., & Cardenas, M. B. (2020). The sensitivity of hyporheic exchange to fractal properties of riverbeds. *Water Resources Research*, 56, e2019WR026560. https://doi.org/10.1029/2019WR026560

Legleiter, C. J. (2014). A geostatistical framework for quantifying the reach-scale spatial structure of river morphology: 1. Variogram models, related metrics, and relation to channel form. *Geomorphology*, *205*, 65-84. https://doi.org/10.1016/j.geomorph.2012.01.016

Leopold, L. B., Wolman, M. G., & Miller, J. P. (1964). *Fluvial processes in geomorphology*. New York, NY: Dover Publications, Inc.

McElroy, B., & Mohrig, D. (2009). Nature of deformation of sandy bed forms, *J. Geophys. Res.*, 114, F00A04, https://doi.org/10.1029/2008JF001220.

MacVicar, B. J., & A. G. Roy (2007), Hydrodynamics of a forced riffle pool in a gravel bed river: 1. Mean velocity and turbulence intensity, *Water Resour. Res.*, 43, W12401, https://doi.org/10.1029/2006WR005272

MacWilliams Jr, M. L., Wheaton, J. M., Pasternack, G. B., Street, R. L. & Kitanidis, P. K. (2006). Flow convergence routing hypothesis for pool-riffle maintenance in alluvial rivers. *Water Resources Research*, 42 (10), W10427. https://doi.org/10.1029/2005WR004391

Martin, R. L., & Jerolmack, D. J. (2013). Origin of hysteresis in bed form response to unsteady flows. *Water Resources Research*, 49, 1314–1333. https://doi.org/10.1002/wrcr.20093

McKean, J.A., Isaak, D.J. and Wright, C.W. (2008), Geomorphic controls on salmon nesting patterns described by a new, narrow-beam terrestrial–aquatic lidar. *Frontiers in Ecology and the Environment*, 6: 125-130. https://doi.org/10.1890/070109

Montgomery, D. R., & Buffington, J. M. (1993). *Channel classification, prediction of channel response, and assessment of channel condition* (p. 84). Seattle: University of Washington.

Movahedi, N., Dehghani, A. A., Schmidt, C., Trauth, N., Pasternack, G. B., Stewardson, M. J., & Halghi, M. M. (2021). Hyporheic exchanges due to channel bed and width undulations. *Advances in Water Resources*, 149, 103857. https://doi.org/10.1016/j.advwatres.2021.103857

Nikora, V. I. (1991). Fractal structures of river plan forms. *Water resources research*, 27(6), 1327-1333. https://doi.org/10.1029/91WR00095

Nikora, V., & Hicks, D. M. (1997). Scaling relationships for sand wave development in unidirectional flow. *Journal of Hydraulic Engineering*, 123(12), 1152–1156. https://doi.org/10.1061/(ASCE)0733-9429(1997)123:12(1152).

Nikora, V. I., Sukhodolov, A. N. & Rowinski, P. M. (1997). Statistical sand wave dynamics in one-directional water flows, *J. Fluid Mech*., 351, 17–39. https://doi.org/10.1017/S0022112097006708

Nogueira, X. R., Pasternack, G. B., Lane, B. A. & Sandoval-Solis, S. (2024) Width undulation drives flow convergence routing in five flashy ephemeral river types across a dry summer subtropical region. *Earth Surface Processes and Landforms*, 49(6), 1890–1913. https://doi.org/10.1002/esp.5805

Palucis, M. C., & Lamb, M. P. (2017). What controls channel form in steep mountain streams?. *Geophysical Research Letters*, *44*(14), 7245-7255. https://doi.org/10.1002/2017GL074198

Pasternack, G. B., Baig, D., Webber, M., & Brown, R. (2018a). Hierarchically nested river landform sequences. Part 1: Theory. *Earth Surface Processes and Landforms*, *43*(12), 2510-2518. https://doi.org/10.1002/esp.4411

Pasternack, G. B., Baig, D., Weber, M. D., & Brown, R. A. (2018b) Hierarchically nested river landform sequences. Part 2: Bankfull channel morphodynamics governed by valley nesting structure. *Earth Surf. Process. Landforms*, 43: 2519–2532. https://doi.org/10.1002/esp.4410.

Pelletier, J. D. (2007). Fractal behavior in space and time in a simplified model of fluvial landform evolution. *Geomorphology*, 91(3-4), 291-301. https://doi.org/10.1016/j.geomorph.2007.04.015

Rodriguez-Iturbe, I., & A. Rinaldo (2001). *Fractal River Basins: Chance and Self-Organization*, Cambridge Univ. Press, Cambridge, U. K.

Sawyer, A. M., Pasternack, G. B., Moir, H. J., & Fulton, A. A. (2010). Riffle-pool maintenance and flow convergence routing observed on a large gravel-bed river. *Geomorphology*, *114*(3), 143-160. https://doi.org/10.1016/j.geomorph.2009.06.021

Singh, A., Lanzoni, S. P., Wilcock, R. & Foufoula-Georgiou, E. (2011). Multi-scale statistical characterization of migrating bedforms in gravel and sand bed rivers. *Water Resour. Res*., 47, W12526. https://doi.org/10.1029/2010WR010122.

Wheaton, J. M., Brasington, J., Darby, S. E., Merz, J., Pasternack, G. B., Sear, D., & Vericat, D. (2010). Linking geomorphic changes to salmonid habitat at a scale relevant to fish. *River Research and Applications,* 26, 469–486. https://doi.org/10.1002/rra.1305

White, J. Q., Pasternack, G. B., & Moir, H. J. (2010). Valley width variation influences riffle-pool location and persistence on a rapidly incising gravel-bed river. *Geomorphology,* 121, 206-221, https://doi.org/10.1016/j.geomorph.2010.04.012

Wiener, J. S., & Pasternack, G. B. (2022). Scale dependent spatial structuring of mountain river large bed elements maximizes flow resistance. *Geomorphology*, *416*, 108431. https://doi.org/10.1016/j.geomorph.2022.108431

Williams, G. P. (1986). River meanders and channel size. *Journal of hydrology*, *88*(1-2), 147-164. https://doi.org/10.1016/0022-1694(86)90202-7

Williams, Z. C., Pelletier, J. D., & Meixner, T. (2019). Self-affine fractal spatial and temporal variability of the San Pedro River, southern Arizona. *Journal of Geophysical Research: Earth Surface*, *124*(6), 1540-1558. https://doi.org/10.1029/2018JF004853

Wyrick, J. R., & Pasternack, G. B. (2014). Geospatial organization of fluvial landforms in a gravel–cobble river: Beyond the riffle–pool couplet. *Geomorphology*, *213*, 48-65. https://doi.org/10.1016/j.geomorph.2013.12.040

Wyrick, J. R. & Pasternack, G. B. (2016). Revealing the natural complexity of topographic change processes through repeat surveys and decision-tree classification. *Earth Surface Processes and Landforms*, 41 (6), 723-737. https://doi.org/10.1002/esp.3854

Thomson, D. J. (1982). Spectrum estimation and harmonic analysis. *Proceedings of the IEEE*, 70, 1055–1096. https://doi.org/10.1109/PROC.1982.12433

Turcotte, D. L. (1997). *Fractals and Chaos in Geology and Geophysics*, Cambridge Univ. Press, Cambridge, U. K.

van der Mark, C. F., Blom, A. & Hulscher, S. J. M. H. (2008). Quantification of variability in bedform geometry. *J. Geophys. Res.*, 113, F03020, https://doi.org/10.1029/2007JF000940.

River Research and Application

Supporting Information for

Spectral slope and coherence quantitatively summarize nested topographic variability patterns in rivers

A. Lee[1*], B. Lane[1], and G. B. Pasternack[2]

[1]Department of Civil and Environmental Engineering, Utah State University; Logan, UT 84322, USA.
[2]Department of Land, Air & Water Resources, University of California, Davis; Davis, CA 95616, USA.

[*]Corresponding author: Anzy Lee (anzy.lee@usu.edu)

Contents of this file

Text S1 to S3
Figure S1 to S4
Table S1 to S4

Introduction

This document describes the methods used for river classification (Text S1), and extraction of width and bed elevation (Text S2). Detailed information on key metric values used for LiDAR data, width and bed elevation extraction are presented in Table S1 and S2. Reach-average river metrics and spectral slopes are given in Table S3, and S4.

Text S1. Site selection and river classification

This study employed a three-way random-stratified sampling methodology to obtain an initial set of representative ephemeral stream reaches to consider for use as study sites in the South Coast region of California. Three sources of pre-existing published information were used to stratify potential study sites. First, reaches had to be classified as having ephemeral hydrology, based on the California hydrologic classification's "Flashy-Ephemeral River (FER)" designation (Lane et al., 2018).

Second, a reach had to be fully covered with a topo-bathymetric point cloud, which is the input data for the algorithms used in this study. Considering the South Coast region of California, streams are often dry for much of the year, so sub-meter-resolution airborne LiDAR surveys (Table S1) alone can yield such complete datasets suitable for the algorithm. In other regions, it would be necessary to perform bathymetric mapping together with topographic mapping. For this study, airborne LiDAR coverage polygons were used to stratify streams on the basis of coverage or no coverage.

Table S1. Key metric associated with utilized dry season (May – October) LiDAR project data.

LiDAR dataset	Mean point spacing (m)	Vertical RMSE (cm)	# of river reaches
2015 Los Angeles County, CA QL2 Lidar	0.7	9.95	2
2018 Southern California Wildfire FEMA R9 QL1 Lidar	0.35	10	17
2018 Southern California Wildfire QL2 Lidar	0.7	5.4	16

Third, a reach had to be initially classified into one of the five South Coast regional river types by Byrne et al. (2020), as this provided the typology to ensure that site selection in this study spanned the diverse river types in the region. River-type prediction had been done on each 200-m length interval along all lines representing streams present in the National Hydrography Dataset version 2 (McKay et al., 2012; NHDPlusV2). Prediction models were made on an ensemble basis using Random Forest, Support Vector Machine, and Artificial Neural Network methods. Training data consisted of river type labels for 67 independent sites subjected to thorough geomorphic characterization spanning the five channel types in the region (Byrne et al., 2020). A total of 147 potential predictors quantifying metrics of river corridor terrain, river network topology, topographic fractal dimension, sediment supply, valley confinement, and contributing drainage area, as detailed in Guillon et al. (2020) and Lane et al. (2021). Among California's regions, the South Coast had the lowest prediction accuracy, but the cross-validated multiclass AUC was still 0.949 and the cross-validated accuracy was > 70%. Among the three modeling methods, the Random Forest model was selected to generate the final river type predictions (Fig. S1). The final classification tree was defined by CV_d (Coefficient of variation of depth), w/d (Width-to-depth ratio), s (Slope), and C_v (Valley confinement). Details on modeling methods and predictive performance are available at https://guillon.xyz/regional_comparison_pRA17Mm/index.html. Noting that statistical methods to create the regional river-type classification had uncertainty arising from a modest number of samples, multivariate classification algorithms, and the final Random Forest machine learning prediction framework, a river type verification/re-assignment process was performed as the last step in the site-selection process after detailed information about each site was available and analyzed, as described below (as that scope of work data processing could not be fully automated and applied to the entire river network at the outset).

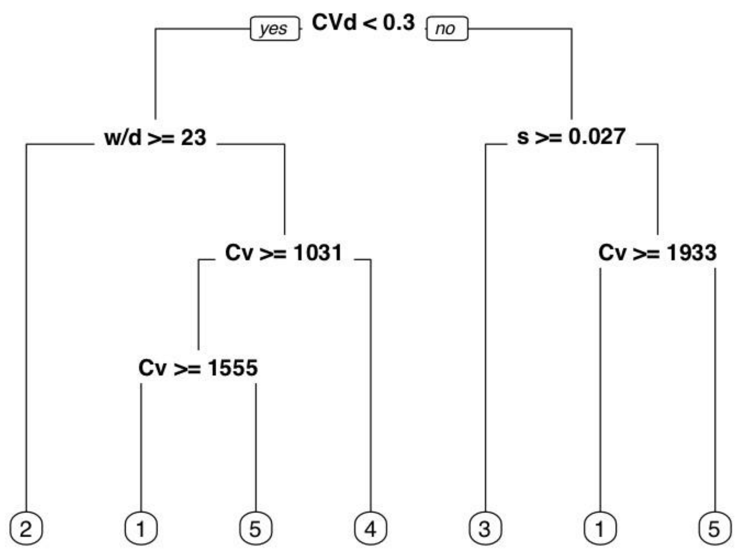

Figure S1. Final yes/no classification tree that produced suitable prediction and cross-validation percentages. Channel types are indicated by numbers at the bottom of the figure.

Text S2. Spectral analysis

Spectral analysis starts by conducting Fourier transforms of longitudinal series of mean-width-normalized wetted width (Wn) and detrended, mean-width-normalized bed elevation (Zn), for key threshold stages evident in a river's topography (e.g., baseflow, bankfull and flood stage). All spectral analysis used seven 4π Slepian multitapers which reduces the variance of the spectral estimate (Thomson, 1982; Lees & Park, 1995). To measure spectral slope, we first identified the slope break where the spectrum shows power-law scaling relationship to the maximum frequency and calculated the slope using linear regression in log-log scale from the slope break to the maximum frequency (Fig. S2a, b).

Thomson's (1982) Fourier-based spectral estimators were used to investigate frequency-based correlations between Wn and Zn at baseflow, bankfull and flood stages (Fig. S2c). A strong correlation between the two series results in high coherency value and vice versa (Fig. S2c, top). We recorded the magnitude-squared coherencies that are dominant or statistically significant satisfying 99% confidence level along with their frequencies and phases (Fig. S2c, bottom) (Carter et al., 1973; Hinnov, 1994; Priestley, 1981).

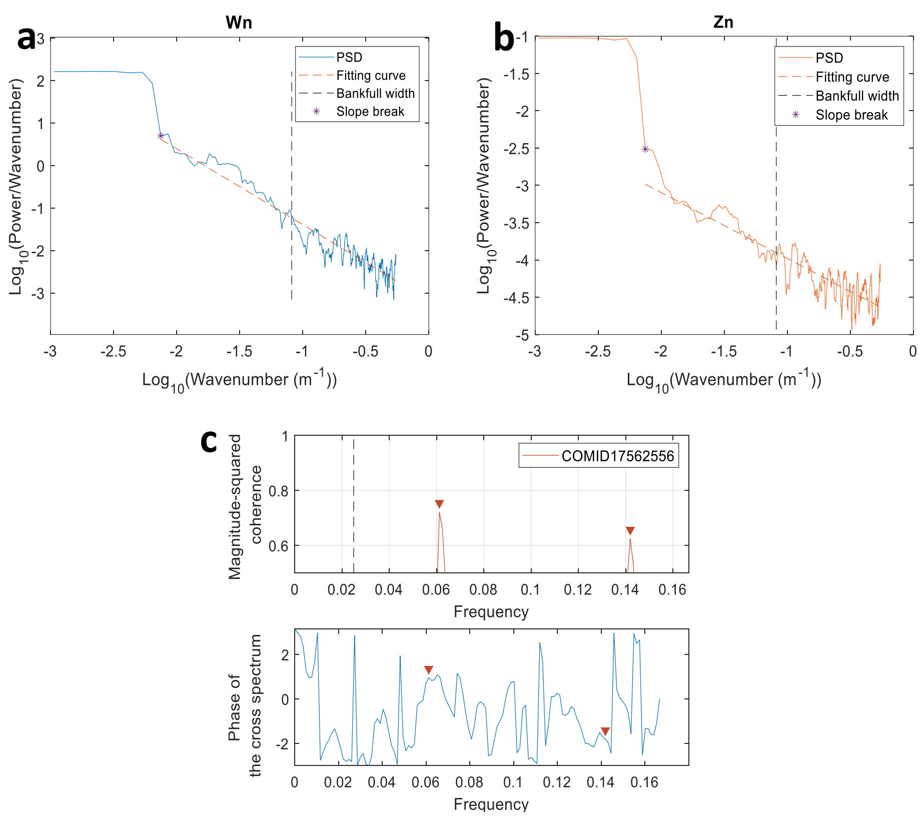

Figure S2. Example multitaper power spectrum density (PSD) estimate and spectral slope of (a) Wn and (b) Zn at bankfull flow for an unconfined, uniform, sand-gravel channel with bankfull width of 12.22 m. (c) Example magnitude-squared coherence (top) and phase of the cross spectrum (bottom) for baseflow stage for an unconfined, uniform, gravel-cobble channel.

Text S3. Extraction of width and bed elevation

After all stream reaches in the South Coast region were subjected to three-way stratification (i.e., FER, lidar coverage, and predicted stream type), then eight study sites were randomly chosen from the population for each river type, yielding 40 candidate study river intervals, each 200-m long. The sites were not considered final, because after selection each site's meter-resolution digital elevation model (DEM) could be generated and analyzed using the geomorphic covariance structure (GCS) graphical user interface (GUI) software (available at https://github.com/xaviernogueira/GCS-Analysis-Tools) to (i) evaluate the suitability of a site for use in the study and (ii) obtain a more accurate river-type classification to re-sort the set of final sites by river type. Inspection of site DEMs found that five sites were unsuitable and therefore removed from the study. For example, unsuitable sites might have artificially dug small reservoirs or engineered confinements (e.g., levees or walls).

After the final set of 35 dry river-corridor sites was selected, the bare-ground elevation point cloud data for each site was clipped to a length judged to be a consistent geomorphic reach type based on expert judgment evaluated by two experts who evaluated multiple years of meter-resolution aerial image available on Google Earth and terrain indicators in the DEM. After clipping, the average study reach length was 56 times mean channel width at bankfull discharge. These spans are substantially long for GCS analysis and are consistent with classic reach length norms (> 10-20 times bankfull width) for reach-scale studies (Nardini et al., 2020).

Airborne LiDAR point cloud data for each site were processed using a novel algorithm that is part of a geomorphic analysis tool (Nogueira et al., 2024) to create each study site's meter-resolution DEM, generate thalweg-detrended DEMs, and extract longitudinal width (W) and bed elevation (Z) for three key flow stage elevations: baseflow, bankfull, and flood stage (Table S2). Further information on the details of these geomorphic analysis can be found in Nogueira et al. (2024).

In addition, the GCS program was used to compute reach-average slope, valley confinement distance, bankfull width to depth ratio, and bankfull depth coefficient of variation (Table S3). These variables were then put into the river-type classification decision tree (Fig. S1) for the South Coast region (Byrne et al., 2020) to verify the river type predicted and assigned by the Random Forest model. Sites found to have a different class than originally predicted were re-assigned to the correct river type class. As a result, two river types only had six sites and one only had seven sites, instead of all sites having eight sites. Additional reach-average terrain metrics for each site were also computed (Table S3).

Sensitivity analysis was conducted to assess the extent to which channel-type sample sizes (i.e., 6, 7, or 8 sites) impacted class-averaged GCS metrics. That analysis found that group sample sizes were sufficient to prevent a single river reach from significantly affecting class-averaged GCS values in this study. Considering that no prior study has analyzed more than a single site's GCS before, having 6-8 per river type with a total of 35 sites was considered a significant, acceptable development for moving forward with the study.

Table S2. Key metric values used width and bed elevation extraction.

River type	COMID	Spatial series interval (m)	Reach length (m)	Baseflow stage height (m)	Bankfull stage height (m)	Flood stage height (m)
1	17573013	1.83	611	0.06	0.67	1.55
1	17573045	1.83	2207	0.18	0.94	3.66
1	17567211	0.91	719	0.03	0.27	0.79
1	17633478	1.83	410	0.03	0.30	0.94
1	17562556	0.91	576	0.09	0.91	N/A
1	17609947	1.83	1271	0.06	0.21	0.79
2	17610671	3.66	1185	0.12	0.82	2.44
2	17586760	3.66	1284	0.21	0.82	1.52
2	17609707	2.74	628	0.15	0.61	1.52
2	17586810	2.74	903	0.18	1.10	2.47
2	17609015	3.66	1156	0.09	1.04	3.14
2	17637906	2.74	1791	0.09	0.37	1.62
3	17594703	0.91	1608	0.15	0.88	1.71
3	17609699	1.83	1042	0.15	0.67	1.71
3	17570395	1.83	1507	0.06	0.34	1.52
3	17609755	0.91	617	0.06	0.30	1.07
3	17586504	0.91	822	0.21	0.88	1.49
3	17570347	0.91	1125	0.18	0.98	1.83
3	17569535	0.91	711	0.27	0.91	1.77
4	17563722	0.91	813	0.21	0.49	1.46
4	17569841	0.91	896	0.09	0.46	1.52
4	17563602	1.83	929	0.18	0.37	1.83
4	17610235	0.91	1915	0.12	0.58	1.16
4	17595173	1.83	682	0.00	0.30	1.40
4	22514218	0.91	454	0.03	0.27	1.58
4	17610257	0.91	902	0.12	0.76	1.49
4	17610541	1.83	1372	0.15	0.70	1.80
5	17585756	1.83	836	0.24	0.61	1.31
5	17611423	1.83	1569	0.24	0.55	1.83
5	17610721	2.74	1772	0.12	0.40	1.25
5	17586610	0.91	774	0.15	0.52	1.65
5	17607455	1.83	439	0.09	0.43	1.28
5	17607553	1.83	1441	0.06	0.34	0.79
5	17609017	2.74	1152	0.15	1.28	2.23
5	17610661	3.66	871	0.15	0.64	2.59

Table S3. Summary table for reach-average river metrics. Avg.: Average, CV: coefficient of variation, W: width, d: depth, W/d: width to depth ratio

River type	COMID	Stream order	Catchment area (km^2)	Valley confinement (m)	Channel slope	CV of W	CV of d	Avg. baseflow d (m)	Avg. baseflow d (m)	Avg. bankfull W (m)	Avg. bankfull d (m)	Avg. flood W (m)	Avg. flood d (m)	Baseflow W/d	Bankfull W/d	Flood w/d
1	17573013	3	23.45	1631.88	0.0047	0.28	0.34	5.24	0.30	38.57	0.83	85.05	1.71	17.69	46.62	49.70
1	17573045	3	37.07	1968.60	0.0043	0.23	0.38	5.98	0.23	19.92	0.92	417.20	3.63	25.76	21.60	114.82
1	17567211	2	6.96	1546.92	0.0036	0.46	0.28	3.75	0.06	9.70	0.23	64.94	0.74	58.19	41.72	87.47
1	17633478	3	40.91	821.67	0.0059	0.39	0.34	5.52	0.06	13.90	0.28	20.33	0.91	88.19	49.01	22.25
1	17562556	2	11.08	1143.25	0.0073	0.15	0.29	4.34	0.13	12.22	0.91	N/A	N/A	32.48	13.36	N/A
1	17609947	3	37.93	576.50	0.0035	0.39	0.74	7.38	0.08	15.87	0.19	31.01	0.77	95.52	82.84	40.36
2	17610671	5	636.40	117.86	0.0024	0.39	0.38	19.39	0.11	70.24	0.60	208.94	2.21	176.48	116.46	94.58
2	17586760	6	209.60	758.00	0.0037	0.18	0.25	30.99	0.17	244.03	0.75	441.08	1.45	182.38	326.42	304.48
2	17609707	3	23.33	401.10	0.0039	0.39	0.40	8.86	0.10	45.87	0.42	86.54	1.33	88.81	108.52	65.12
2	17586810	4	123.58	153.69	0.0029	0.28	0.39	10.66	0.11	51.65	0.83	249.55	2.20	93.53	62.20	113.47
2	17609015	5	1468.03	837.75	0.0015	0.35	0.21	29.68	0.13	224.60	0.67	296.59	2.77	227.19	333.17	106.89
2	17637906	3	99.56	231.60	0.0069	0.31	0.30	25.64	0.08	66.28	0.31	182.47	1.55	339.78	215.39	117.48
3	17594703	2	8.97	18.82	0.0203	0.19	0.39	6.73	0.19	22.13	0.87	40.00	1.69	34.54	25.41	23.61
3	17609699	2	12.78	13.54	0.0269	0.42	0.32	7.76	0.28	19.81	0.68	34.91	1.70	28.20	29.07	20.56
3	17570395	3	21.10	14.00	0.0172	1.51	0.35	5.98	0.15	12.51	0.30	34.14	1.37	39.69	41.75	24.85
3	17609755	2	2.72	12.00	0.0136	0.88	0.37	2.69	0.17	5.15	0.33	14.65	1.02	15.37	15.71	14.34
3	17586504	2	3.03	16.33	0.0518	0.41	0.46	7.45	0.34	19.03	0.88	30.21	1.48	21.71	21.73	20.41
3	17570347	2	2.90	0.86	0.0413	0.40	0.37	5.93	0.33	11.54	0.93	16.70	1.77	18.12	12.43	9.41
3	17569535	2	3.16	41.29	0.0441	0.61	0.51	4.85	0.59	9.11	1.11	17.47	1.94	8.24	8.18	9.03
4	17563722	2	2.14	18.88	0.0119	0.50	0.63	4.54	0.29	12.35	0.51	33.44	1.46	15.40	24.24	22.97
4	17569841	2	6.83	24.57	0.0108	0.88	0.51	7.80	0.15	18.73	0.38	48.34	1.38	50.67	49.05	35.16
4	17563602	2	17.91	94.00	0.0077	0.36	0.00	18.39	0.19	31.90	0.37	130.66	1.83	96.35	86.72	71.39
4	17610235	2	7.43	15.70	0.0120	0.33	0.34	4.73	0.19	13.83	0.56	22.36	1.14	25.38	24.60	19.65
4	17595173	3	12.67	8.14	0.0201	0.76	0.35	9.80	0.32	15.16	0.53	30.26	1.54	30.86	28.66	19.67
4	22514218	2	3.62	24.13	0.0742	0.90	0.66	5.29	0.34	10.42	0.49	22.36	1.71	15.46	21.23	13.06
4	17610257	2	4.42	10.08	0.0296	0.33	0.21	4.66	0.21	10.32	0.73	15.42	1.46	22.55	14.05	10.55
4	17610541	4	84.33	55.00	0.0041	0.13	0.14	12.50	0.15	27.01	0.68	50.14	1.78	84.68	39.67	28.20
5	17585756	3	32.13	73.44	0.0102	0.24	0.28	9.46	0.25	19.85	0.61	42.46	1.31	38.01	32.66	32.44
5	17611423	4	62.26	137.18	0.0041	0.26	0.36	8.97	0.25	26.14	0.53	128.43	1.81	36.08	49.26	70.95
5	17610721	4	89.13	149.40	0.0039	0.49	0.37	11.75	0.11	24.57	0.33	82.15	1.16	104.31	74.83	70.85
5	17586610	2	9.61	828.25	0.0302	0.56	0.12	7.99	0.18	20.88	0.41	47.15	1.51	43.51	51.38	31.16
5	17607455	3	11.66	23.33	0.0132	0.47	0.52	6.10	0.12	13.81	0.36	45.68	1.20	50.83	38.51	38.02
5	17607553	2	13.36	279.00	0.0037	0.47	0.47	4.36	0.09	11.62	0.32	45.30	0.78	47.38	35.76	58.22
5	17609017	4	122.80	169.33	0.0012	0.12	0.31	7.97	0.14	28.16	1.21	43.45	2.16	54.94	23.20	20.13
5	17610661	5	652.81	423.17	0.0012	0.24	0.31	15.76	0.16	42.71	0.59	334.45	2.54	96.35	72.67	131.91

Table S4. Summary table for spectral slopes

River type	COMID	Wn Spectral slope						Zn Spectral slope					
		Baseflow / R^2		Bankfull / R^2		Flood / R^2		Baseflow / R^2		Bankfull / R^2		Flood / R^2	
1	17573013	0.71	0.67	1.95	0.89	2.04	0.89	0.55	0.64	1.43	0.76	1.84	0.85
1	17573045	1.01	0.70	1.59	0.86	2.02	0.87	0.65	0.48	0.98	0.74	2.25	0.90
1	17567211	0.95	0.61	1.41	0.93	2.22	0.85	0.67	0.44	0.85	0.86	1.69	0.90
1	17633478	1.03	0.78	1.01	0.87	1.77	0.87	0.68	0.58	0.95	0.80	1.07	0.72
1	17562556	0.96	0.85	1.79	0.91	N/A	N/A	0.71	0.45	0.88	0.75	N/A	N/A
1	17609947	1.53	0.62	2.12	0.55	2.18	0.83	0.57	0.63	1.09	0.65	1.16	0.79
2	17610671	1.64	0.92	1.81	0.88	2.25	0.84	1.42	0.75	1.55	0.83	1.99	0.87
2	17586760	1.71	0.60	2.08	0.53	2.14	0.88	1.52	0.66	1.82	0.65	2.12	0.79
2	17609707	1.39	0.85	2.34	0.64	2.77	0.76	0.9	0.84	1.74	0.87	1.95	0.78
2	17586810	0.81	0.89	0.97	0.93	2.33	0.89	0.89	0.66	0.98	0.78	2.03	0.87
2	17609015	1.6	0.84	1.31	0.86	1.99	0.90	1.65	0.81	1.58	0.87	1.67	0.85
2	17637906	1.57	0.88	1.7	0.90	2.02	0.90	1.46	0.86	1.61	0.86	1.84	0.92
3	17594703	1.6	0.84	1.7	0.90	2.02	0.94	1.28	0.81	1.28	0.82	1.36	0.90
3	17609699	1.18	0.90	1.43	0.89	1.9	0.90	1.04	0.89	1.37	0.85	1.32	0.82
3	17570395	1.28	0.85	1.26	0.86	1.7	0.90	1.15	0.78	1.42	0.88	1.43	0.88
3	17609755	0.83	0.91	1.15	0.86	1.53	0.92	0.57	0.91	0.51	0.85	0.68	0.83
3	17586504	1.61	0.87	1.62	0.83	2.07	0.90	1.39	0.85	1.31	0.83	1.42	0.77
3	17570347	1.48	0.76	1.64	0.87	1.74	0.87	1.31	0.76	1.27	0.89	1.17	0.84
3	17569535	1.47	0.73	1.73	0.81	1.93	0.90	1.06	0.50	1.11	0.57	1.58	0.64
4	17563722	0.89	0.86	1.37	0.91	1.55	0.93	0.71	0.78	0.84	0.79	1.04	0.88
4	17569841	1.36	0.69	1.58	0.86	1.83	0.84	0.79	0.64	1.03	0.74	1.44	0.74
4	17563602	1.67	0.88	2.11	0.90	2.42	0.87	1.21	0.71	1.28	0.77	1.85	0.87
4	17610235	1.16	0.89	1.56	0.88	1.69	0.87	0.96	0.85	1.13	0.79	1.04	0.78
4	17595173	1.48	0.85	1.58	0.89	1.9	0.88	1.23	0.81	1.11	0.83	1.17	0.76
4	22514218	1.56	0.83	1.75	0.87	1.61	0.86	1.28	0.80	1.16	0.79	1.24	0.78
4	17610257	1.33	0.75	1.33	0.80	1.47	0.93	1.05	0.65	1.08	0.70	1.04	0.80
4	17610541	1.09	0.89	1.43	0.88	2.11	0.79	1.04	0.85	1.01	0.72	1.43	0.82
5	17585756	1.28	0.76	1.58	0.85	2.08	0.94	1.24	0.68	1.26	0.81	1.42	0.77
5	17611423	1.06	0.87	1.62	0.86	1.98	0.91	0.84	0.73	1.11	0.87	1.66	0.81
5	17610721	1.34	0.74	1.62	0.88	2.05	0.93	1.03	0.74	1.27	0.74	1.62	0.89
5	17586610	1.51	0.74	1.59	0.89	2.08	0.93	1.08	0.51	1.34	0.77	1.4	0.85
5	17607455	1.13	0.86	1.92	0.85	1.83	0.85	0.9	0.66	1.2	0.84	1.71	0.83
5	17607553	0.88	0.64	1.81	0.81	2.26	0.93	0.56	0.81	0.92	0.82	1.7	0.85
5	17609017	1.23	0.86	1.74	0.87	2.09	0.91	0.9	0.70	1.44	0.82	1.74	0.88
5	17610661	1.04	0.81	1.6	0.87	2.53	0.88	1.3	0.67	1.4	0.84	1.97	0.85

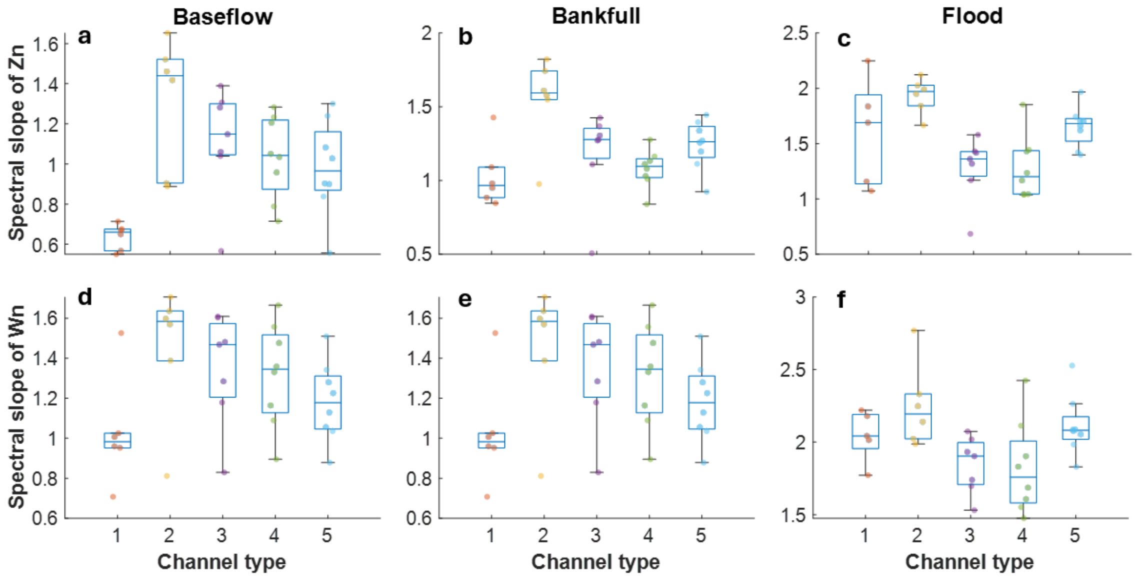

Figure S3. The spectral and a scatter plot of Zn and Wn spectral slopes with respect to channel type. The box chart displays the median, lower and upper quartiles, any outliers (computed using the interquartile range), and the non-outlier minimum and maximum values.

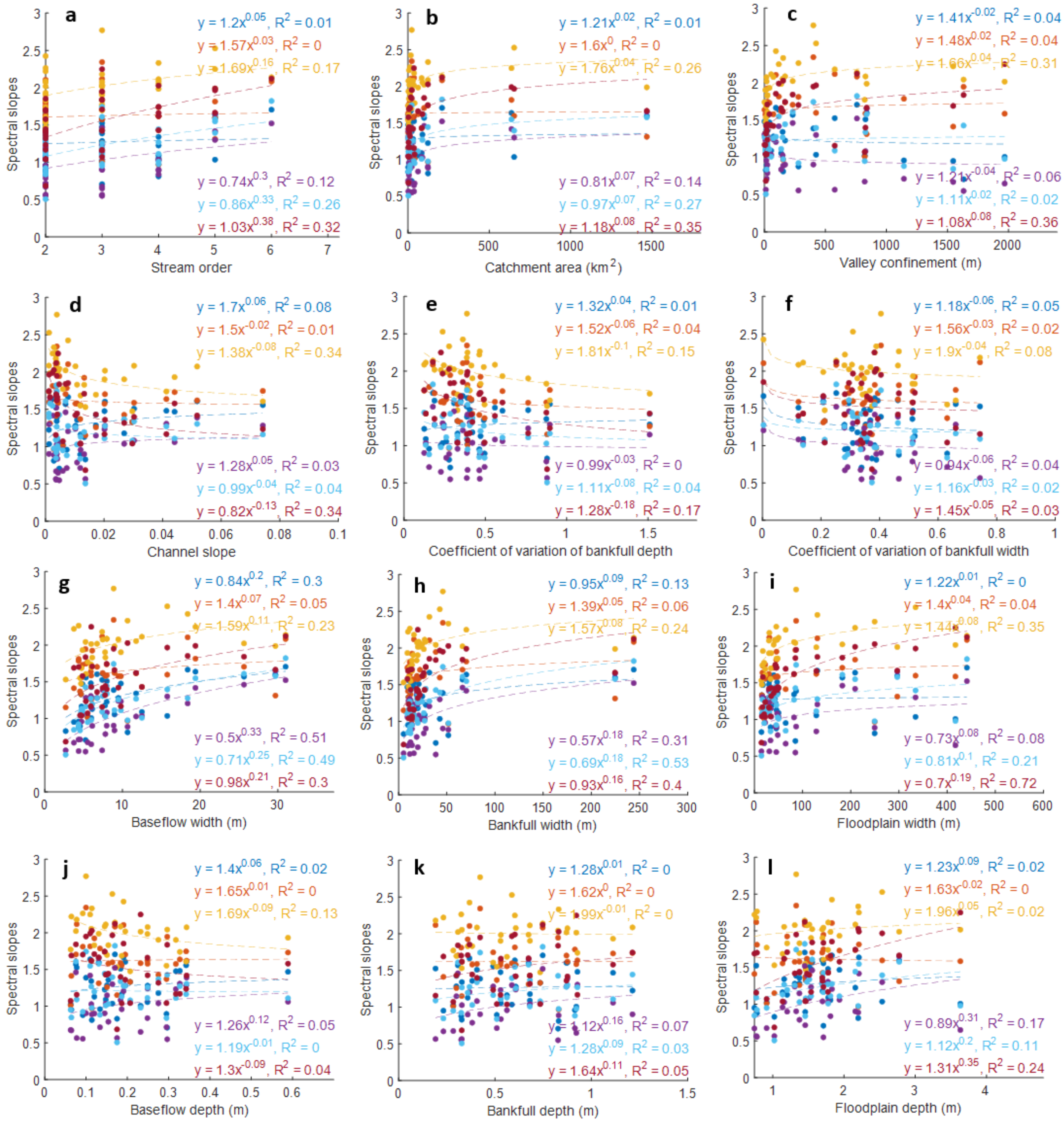

Figure S4. The spectral slope of width (blue/orange/yellow dots) and bed elevation (purple/light blue/red dots) for baseflow/bankfull/flood stages versus (a) stream order, (b) catchment area, (c) valley confinement, (d) channel slope, (e) coefficient of variance of bankfull depth, (f) coefficient of variance of bankfull width (g) baseflow width, (h) bankfull width, (i) floodplain width, (j) baseflow depth, (k) bankfull depth, and (l) floodplain depth. Dashed lines are corresponding power-law fitting curves.

References

Byrne, C. F., Guillon, H., Lane, B. A., Pasternack, G. B., & Sandoval-Solis, S. (2020). *Coastal California Regional Geomorphic Classifications*. Prepared for the California State Water Resources Control Board. University of California, Davis, CA.

Carter, G. C., Knapp, C. H., & Nuttall, A. H. (1973). Estimation of the magnitude-squared coherence function via overlapped Fast Fourier transform processing. *IEEE Transactions on Audio and Electroacoustics*, 21, 337–344. https://doi.org/10.1109/TAU.1973.1162496

Guillon, H., Byrne, C. F., Lane, B. A., Sandoval Solis, S., & Pasternack, G. B. (2020). Machine learning predicts reach-scale channel types from coarse-scale geospatial data in a large river basin. *Water Resources Research*, *56*(3), e2019WR026691. https://doi.org/10.1029/2019WR026691

Hinnov, L. A. (1994). *Astronomical forcing, ancient climatic change, and the sedimentary record*. PhD thesis. Baltimore, MD: The Johns Hopkins University.

Lane, B. A., Pasternack, G. B., & Sandoval-Solis S. (2018) Integrated analysis of flow, form, and function for river management and design testing. *Ecohydrology*, 11, e1969. https://doi.org/10.1002/eco.1969

Lane, B. A., Guillon, H., Byrne, C. F., Pasternack G. B., Rowles, J., & Sandoval-Solis, S. (2021). Channel reach morphology and landscape properties are linked across a large heterogeneous region. *Earth Surface Process and Landforms*. https://doi.org/10.1002/esp.5246

Lees, J. M., & Park, J. (1995). Multiple-taper spectral analysis: A stand-alone C-subroutine. *Computers & Geosciences*, 21(2), 199-236. https://doi.org/10.1016/0098-3004(94)00067-5

McKay L., Bondelid T., & Dewald T. (2012). NHDPlus Version 2: User Guide. U.S. EPA and USGS.

Nardini, A., Yépez, S., Mazzorana, B., Ulloa, H., Bejarano, M. D. & Laraque, A. (2020). A systematic, automated approach for river segmentation tested on the Magdalena River (Colombia) and the Baker River (Chile). *Water, 12*(10), p.2827. https://doi.org/10.3390/w12102827

Nogueira, X. R., Pasternack, G. B., Lane, B. A. & Sandoval-Solis, S. (2024) Width undulation drives flow convergence routing in five flashy ephemeral river types across a dry summer subtropical region. *Earth Surface Processes and Landforms*, 49(6), 1890–1913. https://doi.org/10.1002/esp.5805

Priestley, M. B. (1981). *Spectral analysis and time series* (890 pp.). London: Academic Press.

Sear, D. A. (1996). Sediment transport processes in pool–riffle sequences. *Earth Surface Processes and Landforms*, *21*(3), 241-262. https://doi.org/10.1002/(SICI)1096-9837(199603)21:3<241::AID-ESP623>3.0.CO;2-1

Thomson, D. J. (1982). Spectrum estimation and harmonic analysis. *Proceedings of the IEEE*, 70, 1055–1096. https://doi.org/10.1109/PROC.1982.12433